FERMILAB-PUB-09-632-T

# Global interpretation of direct Dark Matter searches after CDMS-II results

**Joachim Kopp**,[1,*] **Thomas Schwetz**,[2,†] and **Jure Zupan**[3,4,‡]

[1] *Theoretical Physics Department, Fermi National Accelerator Laboratory, P.O. Box 500, Batavia, IL60510, USA*
[2] *Max-Planck-Institute for Nuclear Physics, PO Box 103980, 69029 Heidelberg, Germany*
[3] *Faculty of mathematics and physics, University of Ljubljana, Jadranska 19, 1000 Ljubljana, Slovenia*
[4] *Josef Stefan Institute, Jamova 39, 1000 Ljubljana, Slovenia*



## Abstract

We perform a global fit to data from Dark Matter (DM) direct detection experiments, including the recent CDMS-II results. We discuss possible interpretations of the DAMA annual modulation signal in terms of spin-independent and spin-dependent DM–nucleus interactions, both for elastic and inelastic scattering. We find that for the spin-dependent inelastic scattering off protons a good fit to all data is obtained. We present a simple toy model realizing such a scenario. In all the remaining cases the DAMA allowed regions are disfavored by other experiments or suffer from severe fine tuning of DM parameters with respect to the galactic escape velocity. Finally, we also entertain the possibility that the two events observed in CDMS-II are an actual signal of elastic DM scattering, and we compare the resulting CDMS-II allowed regions to the exclusion limits from other experiments.

In this arXiv version of the manuscript we also provide in appendix A the updated fits including recent CoGeNT results.

*Electronic address: jkopp AT fnal.gov
†Electronic address: schwetz AT mpi-hd.mpg.de
‡Electronic address: jure.zupan AT cern.ch

## I. INTRODUCTION

Direct detection of Dark Matter (DM) relies on signals due to energy deposited from DM recoiling on matter in a detector. The DAMA collaboration has provided strong evidence for an annually modulated signal in the scintillation light from sodium iodine detectors. The combined data from DAMA/NaI [1] (7 annual cycles) and DAMA/LIBRA [2] (4 annual cycles) with a total exposure of 0.82 ton yrs shows a modulation signal with $8.2\,\sigma$ significance. The phase of this modulation agrees with the assumption that the signal is due to the scattering of Weakly Interacting Massive Particles (WIMPs) forming the DM halo of our Galaxy.

After a series of experiments with negative results, the CDMS collaboration has recently presented an analysis where 2 events over an expected background of $0.9 \pm 0.2$ events have been seen after 612 kg days of exposure [3]. The probability to observe two or more background events is 23%, which means that the two events neither provide a statistically significant evidence for DM interactions nor can they be rejected as a background. In this paper we investigate both hypotheses and confront them with the results of the other DM direct detection experiments. Another recent direct detection result is due to XENON10 [4] that is searching for signs of DM scattering on liquid xenon. In a recent re-analysis [5] of their 316.4 kg day exposure they found 13 events with expected background of 7.4 events, which was used to set limits on DM scattering cross sections.

Both of these very recent experimental results merit re-examination of the DAMA signal and its consistency with the results from the other direct detection experiments. In the present manuscript we address the following questions:

- Is it possible to reconcile the DAMA annual modulation signal with the constraints from all other experiments?
- If interpreted as DM signal, are the two events observed in CDMS consistent with results of other experiments?

We will focus on four classes of DM scattering cross sections that cover a large set of DM models: the spin-dependent (SD) and spin-independent (SI) WIMP–nucleon scattering that can be either elastic or inelastic. We will use the shorthand notations eSD, eSI, iSD, iSI, to denote these four classes.

Part of the answer to the first question is already well known from the literature, since many of the interpretations of the DAMA signal are in conflict with the constraints from other DM direct detection experiments. For instance, recent analyses of the eSI case have been performed in [6–14]. We will show that this scenario gets even more disfavoured due to the new CDMS and XENON10 results. Similarly, the explanation of the DAMA signal due to the elastic spin-dependent scattering (eSD) is disfavoured by the strong constraints from COUPP [15], KIMS [16], and PICASSO [17].

The case of inelastic spin-independent (iSI) scattering of a DM particle to a nearly degenerate excited state [18] is also tightly constrained, especially by CRESST-II [19] and ZEPLIN-III [20], c.f. recent analyses [21–26]. However, as we will show, the spin-dependent inelastic scattering (iSD) offers a viable explanation of the DAMA signal, consistent with all other constraints. To the best of our knowledge, this solution to DAMA has not been discussed in the literature before.

Unlike DAMA the CDMS signal is statistically very weak. Even so, focusing on the second question above, we also entertain the hypothesis that the two events in CDMS are indeed due to DM and perform a maximum likelihood fit allowing for the presence of a signal. In the case of elastic scattering (eSI and eSD) we obtained a very weak (at the $1\sigma$ level) indication for a positive DM signal, and compare the corresponding allowed regions to the constraints from all other experiments.

The outline of the paper is as follows. In section II we collect expressions for predicted event rates in DM scattering experiments, in section III we describe details of individual experiments relevant for the combined analysis, while in section IV we then give the results of the fits. A simple DM toy model leading to inelastic spin-dependent scattering is presented in section V, followed by conclusions in section VI. In appendix we also include the interpretation of most recent CoGeNT result that appeared after the publication of the manuscript.

In addition to the four general classes of DM models considered in this work, there are also other proposals to explain the DAMA signal, including for example mirror world DM [27], DM with electric or magnetic dipole moments [28], leptophilic DM [29], resonant DM–nucleus scattering [30], modified scattering due to DM form factors [31, 32], and atomic DM [33]. The implications of the new CDMS results for the above models is an interesting open question that, however, is beyond the scope of this paper.

## II. EVENT RATES

The differential counting rate in a direct DM detection experiment (in units of counts per energy per kg detector mass per day) is given by

$$\frac{dR}{dE_d} = \frac{\rho_0}{m_\chi}\frac{\eta}{\rho_{\rm det}} \int_{v>v_{\rm min}} d^3v \, \frac{d\sigma}{dE_d}\, v f_\odot(\mathbf{v}) \,, \tag{1}$$

where $E_d$ is the energy deposited in the detector, $\rho_0$ is the local DM density (which we take to be 0.3 GeV cm$^{-3}$), $\eta$ is the number density of target particles, $\rho_{\rm det}$ is the mass density of the detector and $d\sigma/dE_d$ is the differential cross section for scattering on a target nucleus. If the target contains different elements (like in the case of the DAMA NaI crystals), the sum over the corresponding counting rates is implied.

In eq. (1), $f_\odot(\mathbf{v})$ is the local WIMP velocity distribution in the rest frame of the detector, normalized according to $\int d^3v\, f_\odot(\mathbf{v}) = 1$. It follows from the DM velocity distribution in the rest frame of the galaxy, $f_{\rm gal}(\mathbf{v})$, by a Galilean transformation with the velocity of the Sun in the galaxy and the motion of the Earth around the Sun. For $f_{\rm gal}(\mathbf{v})$ we assume the conventional Maxwellian distribution with $\bar{v} = 220\,{\rm km\,s^{-1}}$ and a cut-off due to the escape velocity from the galaxy of $v_{\rm esc} = 650\,{\rm km\,s^{-1}}$: $f_{\rm gal}(\mathbf{v}) \propto \exp(-\mathbf{v}^2/\bar{v}^2) - \exp(v_{\rm esc}^2/\bar{v}^2)$ for $v \le v_{\rm esc}$ and zero for $v > v_{\rm esc}$. The precise value of the escape velocity has a negligible impact on our results for elastic scattering, while in the inelastic case the precise shape of the tails of the velocity distribution is important [34], see the discussion in sec. IV.

The lower limit of the integration in eq. (1) is set by the minimal velocity $v_{\rm min}$ that the incoming DM particle has to have in order to be able to deposit an energy $E_d$ in the detector.

For the case of inelastic $\chi N \to \chi' N$ scattering it is given by

$$v_{\rm min} = \frac{1}{\sqrt{2 m_N E_d}} \left( \frac{m_N E_d}{\mu_{\chi N}} + \delta \right), \tag{2}$$

where $\mu_{\chi N} = m_\chi m_N/(m_\chi + m_N)$ is the reduced mass of the nucleus–DM system, with $m_N$ and $M_\chi$ the nucleus and DM masses respectively, while $\delta$ is the mass difference between $\chi'$ and $\chi$. The same equation also applies to elastic $\chi N \to \chi N$ scattering, with $\delta = 0$. As observed in ref. [18] for appropriately chosen $\delta$ one can suppress the signal in experiments where DM scatters on lighter nuclei, while not significantly affecting the rate in DAMA (see also [35, 36]). Namely for $\delta \gg m_N E_d/\mu_{\chi N}$ the minimal velocity $v_{\rm min}$ falls with $m_N$. If the signal is coming from the tails of the velocity distributions, the difference between lighter and heavier nuclei, such as germanium vs. iodine, can be significant (for $v_{\rm min} > v_{\rm esc}$ the scattering is completely absent). Furthermore, the inelasticity also suppresses the low energy signal, changing the shape of the expected event rate from an exponentially falling function of the recoil energy to a bump-like signal at higher energies. This, in addition, improves the fit to the DAMA modulated signal energy spectrum.

The differential cross section for scattering on a target nucleus is (per assumption) given by the spin independent (SI) and spin dependent (SD) contributions, which are conventionally written as (see e.g. [37])

$$\frac{d\sigma}{dE_d} = \frac{m_N}{2\mu_{\chi N}^2 v^2} \left( \sigma^{\rm SI} F^2(E_d) + \sigma^{\rm SD} S(E_d) \right), \tag{3}$$

where $\sigma^{\rm SI,SD}$ are the integrated SI and SD cross sections for DM scattering on nucleus, but with form factors factored out. For the SI form factor $F(E_d)$ we use [38] $F(E_d) = 3e^{-\kappa^2 s^2/2}[\sin(\kappa r) - \kappa r \cos(\kappa r)]/(\kappa r)^3$, with $s = 1$ fm, $r = \sqrt{R^2 - 5s^2}$, $R = 1.2A^{1/3}$ fm, $\kappa = \sqrt{2 m_N E_d}$ (and $q^2 \simeq -\kappa^2$). The SD form factor $S(E_d)$ is computed according to ref. [39] for $^{133}$Cs (abundant in the CsI crystals used by the KIMS experiment) and according to ref. [40] for all other nuclei.

Even though the form factors were factored out of the definitions of $\sigma^{\rm SI,SD}$, these quantities still depend on nuclear structure through isospin content (the number of protons vs. neutrons). The SI cross section is thus

$$\sigma^{\rm SI} = \frac{[Z f_p + (A - Z) f_n]^2}{f_p^2} \frac{\mu_{\chi N}^2}{\mu_{\chi p}^2} \sigma_p^{\rm SI}, \tag{4}$$

with A the atomic mass number, Z the charge of the nucleus, $f_{p,n}$ the SI DM couplings to proton and neutron respectivelly, $\mu_{\chi p}$ the reduced DM–proton mass, and $\sigma_p^{SI}$ the SI cross section for scattering of DM on a proton. In the fits we will assume $f_p = f_n$ for definiteness and quote results in terms of $\sigma_p^{\rm SI}$. Since the ratio $A/Z$ is similar for different nuclei this choice mostly affects only the overall value of $\sigma_p^{SI}$, while it does not affect the relative sizes of contributions from different experiments. It is easy to rescale our results for different values of $f_p$ and $f_n$ through $\sigma_p^{SI} \to \sigma_p^{SI}/(Z/A + (1 - Z/A) f_n/f_p)^2$.

The SD cross section depends in addition on the spin $J$ of the nucleus

$$\sigma^{\rm SD} S(E_d) = \frac{4\mu_{\chi N}^2 \pi}{3\mu_{\chi p}^2 a_p^2 (2J+1)} [a_0^2 S_{00}(q) + a_0 a_1 S_{01}(q) + a_1^2 S_{11}(q)] \sigma_p^{\rm SD}, \tag{5}$$

where $a_0 = a_p + a_n$ and $a_1 = a_p - a_n$ are combinations of the DM couplings to protons $a_p$ and neutrons $a_n$, and $S_{00}(q)$, $S_{01}(q)$, $S_{11}(q)$ are the spin-dependent nuclear structure functions, which we compute according to [39] for $^{133}$Cs and according to [40] for all other nuclei. In the fits we will assume $a_p = 1, a_n = 0$, a choice that leads to a good fit of data. The reason is that a spin-dependent interaction couples predominantly to un-paired nucleons. Hence, for coupling only to protons DAMA can be compatible with the remaining experiments since $^{127}$I has odd $Z$, but even $N$ (i.e., one unpaired proton), while $^{73}$Ge, $^{129}$Xe, $^{131}$Xe all have unpaired neutrons but even $Z$. For the other extreme choice $a_p = 0, a_n = 1$ the DAMA signal is safely incompatible with the other searches, see e.g. [12]. Simultaneous couplings to proton and neutrons can still be allowed, depending on the relative size of the two couplings.

## III. DESCRIPTION OF EXPERIMENTS AND ANALYSIS METHODS

In our fits we use the most sensitive experimental data sets available to date, coming from the experiments DAMA/LIBRA, CDMS-II, XENON10, ZEPLIN-III, CRESST-II, KIMS, and PICASSO. In this section we describe each experiment in turn and comment on the sensitivity to each of the four classes of DM interactions – eSI, eSD, iSI, iSD.

### A. DAMA

In 2008, the DAMA collaboration has published results of the combined DAMA/NaI and DAMA/LIBRA experiments [1, 2], corresponding to an exposure of 0.82 ton yr for a target consisting of radiopure NaI(Tl) crystals. They observe an annual modulation in the signal,

$$S(E,t) = S_0(E) + A(E)\cos\omega(t - t_0)\,, \tag{6}$$

where $\omega = 2\pi/1$ yr, $t_0 = 152$ days. In the fit we use the signal region from 2 to 8 keVee of the spectrum from the combined DAMA/NaI and DAMA/LIBRA ("DAMA", for brevity) data given in fig. 9 of [2], divided into 12 bins. The data points above 8 keVee are consistent with no modulation. Since no signal is predicted in that range from our DM models, they do not provide an additional constraint on the fit, and are thus ignored. Our analysis of the DAMA data is analogous to the one presented in [11, 29].

The signal in DAMA is the energy deposited in scintillation light, while the scattered nucleus is loosing energy both electromagnetically and through nuclear interactions (phonon excitations). This effect is taken into account by the quenching factors that convert the total nuclear recoil energy $E_d$ to the energy seen in the event by the experiment, $q \times E_d$, with units of equivalent electron energy (keVee). For DAMA $q_{\rm Na} = 0.3$ and $q_{\rm I} \simeq 0.09$ [41]. It is, however, known [42, 43] that some recoil nuclei, namely those travelling along the crystal planes, will *not* suffer from quenching, but deposit essentially all their energy electromagnetically (corresponding to $q = 1$). The fraction of recoil nuclei for which this happens has been calculated in [43], but this calculation leaves room for some debate [14, 44, 45], since the channeling effect has not been measured in the relevant energy range so far. In the following we will discuss to what extent possible explanations of the global data rely on the presence of the channeling effect.

For the fit to the DAMA data we construct a $\chi^2$ function from the annually modulated part of the signal

$$\chi^2_{\rm DAMA}(m_\chi, \sigma_p) = \sum_{i=1}^{12} \left( \frac{A_i^{\rm pred}(m_\chi, \sigma_p) - A_i^{\rm obs}}{\sigma_i} \right)^2 , \tag{7}$$

where the sum is over the energy bins, and $A_i^{\rm obs}$ ($\sigma_i$) are the experimental data points (errors) in figure 9 of [2]. We also impose a constraint that the predicted unmodulated signal $S_0$ from DM scattering should not exceed the one measured by DAMA (which consists of background and signal) for any given energy bin. A recent simulation provides a background estimate for DAMA [46]. While this information could be useful for future more refined fits, we take at this point a conservative approach and let the background float freely in the fit.

We find the best fit point by minimising eq. (7) with respect to WIMP parameters. Allowed regions in the $(m_\chi, \sigma_p)$ plane for elastic scattering or in the $(m_\chi, \sigma_p, \delta)$ space for inealstic scattering at a given CL are obtained by looking for the contours $\chi^2(m_\chi, \sigma_p) = \chi^2_{\rm min} + \Delta\chi^2({\rm CL})$, where $\Delta\chi^2({\rm CL})$ is evaluated for the corresponding degrees of freedom (dof), e.g., $\Delta\chi^2(90\%) = 4.6$ or $\Delta\chi^2(99.73\%) = 11.8$ for 2 dof.

### B. CDMS-II

The most recent analysis of CDMS-II was performed on data taken between July 2007 and September 2008 in four periods. Only Ge detectors were used for the DM search with a total exposure of 612 kg days. Two events were seen in the 10–100 keV energy window, with recoil energies of 12.3 keVnr and 15.5 keVnr[1], while $0.8 \pm 0.1 \pm 0.2$, $0.04^{+0.04}_{-0.03}$ and 0.03–0.06 background events are expected from misidentified surface events, cosmogenic background and neutron contamination, respectively. In our fits we take into account that the signal efficiency drops from 32% at 20 keVnr to 25% at both 10 keVnr and 100 keVnr by linear extrapolation. We also include the previous CDMS search with null result for exposure of 397.8 kg days obtained between October 2006 and July 2007 [47]. We use a constant energy resolution of 0.2 keV for the CDMS germanium detectors.

In most part of our work we follow the CDMS collaboration and use the data only to set an upper bound on a possible signal from DM. To this aim we employ Yellin's maximum gap method [48], which by construction leads only to a bound (and never to a positive signal), without any assumptions on the possible origin (background or signal) of observed events. Only in sec. IV B we are more speculative, and perform a maximum likelihood fit to the two observed events assuming a model for the background (details of that analysis are given in sec. IV B).

[1] Here, keVnr refers to the actual *nuclear* recoil energy, as opposed to the equivalent electron energy reported by DAMA.

### C. XENON10

The XENON10 experiment ("XENON", for short) searches for DM scattering on xenon nuclei by measuring simultaneously the scintillation and ionization signals in purified liquid xenon. Using a fiducial mass of 5.4 kg they collected a data sample of 316.4 kg day between October 6, 2006 and February 14, 2007 [4]. The latest analysis [5] of this data yields 13 events with an expected background of 7.4 in the 2.0–75.0 keVnr window. This is a re-analysis of the same data used in [4], where 10 events had been found in a smaller energy window from 4.5–26.9 keVnr. There is still some controversy concerning the effective light yield in liquid xenon, which is needed to translate the observed ionization signal into a nuclear recoil energy [49, 50]. In our analysis, we use the correction factors from [49], but we also discuss the impact of using instead the data from [50]. For the detection efficiency and background estimates, we use the numbers given in table I of [5]. The energy resolution is computed according to [12]

$$\frac{\sigma_E}{E} = \alpha \sqrt{\frac{\mathrm{keV}}{E}} + \beta \tag{8}$$

with $\alpha = 0.579$ and $\beta = 0.021$. We analyze the XENON data using the maximum gap method [48].

### D. ZEPLIN-III

Like XENON10, the ZEPLIN-III experiment is also a two-phase liquid xenon time projection chamber experiment that has accumulated an exposure of 847 kg days between February 27th and May 20th 2008 [51]. They observed 7 events in the 2–16 keVee energy window (shown in fig. 16 of [51]), which corresponds to the nuclear recoil energy window of 10.7–30.2 keVnr. In our analysis we convert keVee into keVnr (and vice-versa) using the scintillation light yields from fig. 15 of [51]. The detection efficiency is taken from fig. 14 of [51], and the energy resolution is assumed to be the same as in XENON10, eq. (8). We analyze the data by employing the maximum gap method.

### E. CRESST-II

The commissioning run of CRESST-II [19] from March 27th to July 23rd, 2007 has a cumulative exposure of 47.9 kg days on $CaWO_4$ crystals. Following [19], we use only tungsten recoils in our analysis. There are 3 events in the 10–40 keVnr energy window at about 17 keVnr, 18 keVnr, and 33 keVnr. We assume a constant efficiency of 90% and a constant energy resolution of 1 keV [25]. For the statistical analysis, we again employ the maximum gap method.

### F. KIMS

The KIMS experiment has an exposure of 3409 kg days taken with low background CsI(Tl) crystals [16]. Since no information on the actual running periods was available to us, we

assume them to be equally distributed throughout the year. We compute the energy resolution according to eq. (8) with $\alpha = 0.582$ and $\beta = 0.0021$ [52] and assume the detection efficiency to be 30% at 3 keVee and 60% at 5 keVee [53]. Between these two energies, we use linear interpolation. The quenching factor is computed from a fit to fig. 4 of [52]. The KIMS data is reported in a window ranging from 3 keVee to 11 keVee, divided into eight bins for each of the four detector modules. We use the $\Delta\chi^2$ method to analyze this data in the same way as the unmodulated DAMA data. To be conservative, we add penalties to the $\chi^2$ only where the predicted event rate is larger than the measured one, in order to make sure that only an upper bound is obtained.

### G. PICASSO

The PICASSO experiment at SNOLAB [17] is very different from the other experiments considered in this work because it is based on the superheated droplet (bubble chamber) technique to search for DM recoiling on $^{19}$F nuclei in a $C_4F_{10}$ target. As we will see below, scattering on $^{19}$F is very sensitive to SD interactions. The experimental procedure is to measure the bubble formation rate as a function of the temperature $T$. Since bubble formation is possible only above a certain threshold energy $E_{\rm thr}$ which depends on $T$ and on the particle species, a DM signal would manifest itself as an increase in the bubble formation rate over a certain $T$ interval. We compute $E_{\rm thr}$ according to eq. (2) of [17]. The PICASSO data, corresponding to a total exposure of $13.75 \pm 0.48$ kg days, is analyzed separately for the two best detectors (modules 71 and 72) with the $\Delta\chi^2$ method, where the background is assumed to have the form $a[1 + \tanh b(T - T_0)]/2.0$, and $a$, $b$, and $T_0$ are free parameters determined by the fit. We also allow for a 14% uncertainty in the predicted signal [17].

## IV. RESULTS

In this section we present the results of our fits to the data. We discuss elastic SI and SD scattering in sec. IV A, and inelastic SI and SD scattering in sec. IV C. While in those two subsections we follow the CDMS collaboration and use their latest data only to set upper limits, in sec. IV B we become more speculative and discuss a possible interpretation of the two observed events as a signal from SI or SD elastic DM scattering.

### A. Elastic SI and SD scattering

In fig. 1, we summarize our results for elastic scattering. We show the DAMA allowed regions compared to constraints from other experiments in the plane of DM mass $m_\chi$ and the interaction cross section for SI scattering and SD scattering off protons. We observe that in both cases the DAMA regions are excluded by the bounds. For the SI case (left panel) the most important bounds come from CDMS and especially from XENON. They exclude the DAMA regions regardless of the assumptions on channeling at high CL. Let us note that for the DAMA region around 10 GeV without channeling additional contraints from CDMS data on silicon apply (not shown) [11].

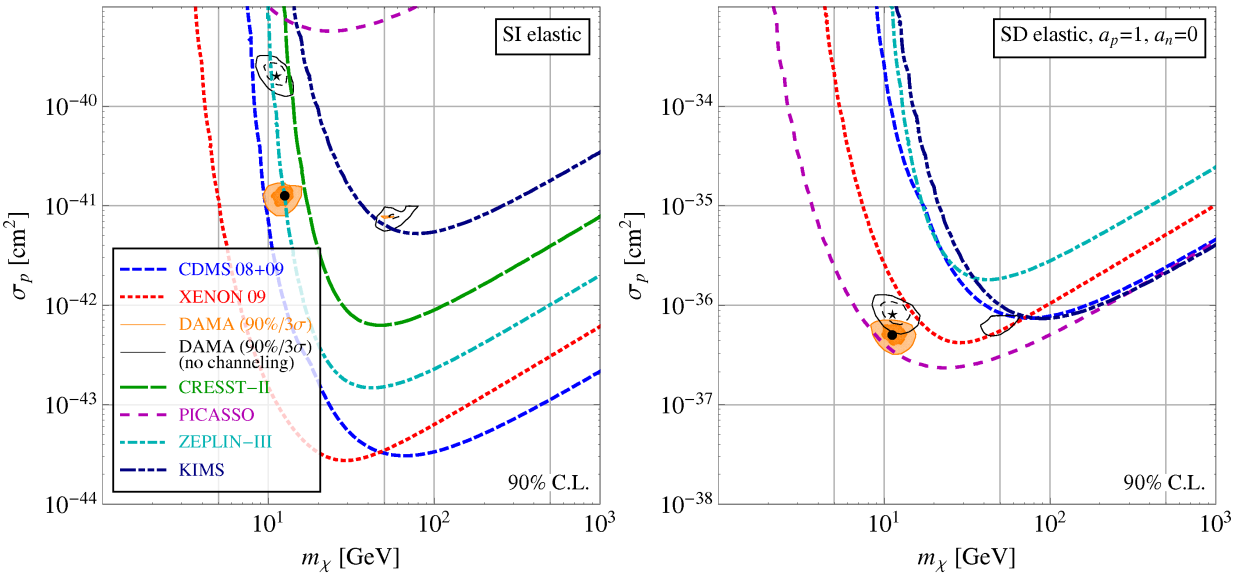


**FIG. 1**: DAMA allowed regions (90% and $3\sigma$ CL) and constraints from other experiments (90% CL) for SI scattering (left) and SD scattering off protons (right). Shaded DAMA regions have been obtained assuming the channeling effect according to [43], while the black contour curves correspond to no channeling.

To study the impact of the new 2009 analyses from XENON [5] and CDMS [3], we compare in fig. 2 the old and new data sets, and show also the impact of different assumptions on the effective light yield $L_{\rm eff}$ in XENON. We observe that despite the large exposure, the new CDMS data has very small impact on the lower bound on $m_\chi$. The reason is that the two observed events are located at low energies, which are most relevant if $m_\chi$ is small, and therefore the maximum gap method leads to a not so strong limit. The new CDMS data is more important if $m_\chi$ is large so that a signal is expected also at larger recoil energies, where no events have been observed. Therefore, thanks to the large exposure the limit improves. We also note a rather significant improvement in the low-mass limit from XENON due to the 2009 analysis. There are two reasons for this effect: first, the energy threshold has been lowered from 4.6 keVnr [4] to 2 keVnr [5], and second, the one event located close to 4.6 keVnr in the 2007 analysis has been eliminated in the 2009 analysis. This leads to a large energy interval at low recoil energies without events, which improves the limit for low masses.

Considering the case of SD elastic DM–nucleus scattering (right panel of fig. 1), we observe that rather strong constraints come from PICASSO, if DM couples mainly to protons ($a_p = 1$, $a_n = 0$). Assuming channeling according to [43] the DAMA region at 90% CL is excluded by the 90% CL bound from PICASSO, while both experiments are marginally compatible at $3\sigma$. Without the channeling effect, there is no overlap of allowed regions. We do not show the case of SD scattering off neutrons ($a_p = 0$, $a_n = 1$), since in that case the DAMA region is safely excluded by CDMS and XENON [12], see also fig. 3. The reason is that the $^{19}$F nuclei in the PICASSO experiment have an unpaired proton, while the spin-

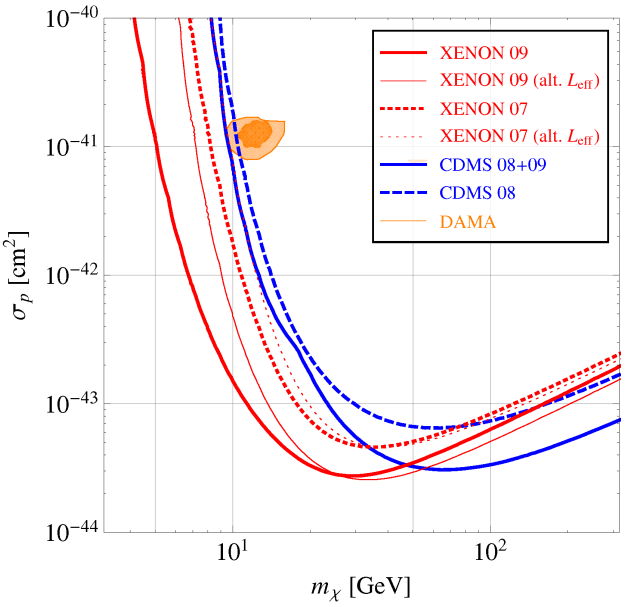


**FIG. 2**: Comparison of different data sets for CDMS and XENON for SI elastic scattering. XENON 07 refers to the analysis from [4], while XENON 09 corresponds to the re-analysis of the same data from [5]. The CDMS 2008 and 2009 data sets are from [47] and [3], respectively. For XENON, different assumptions on the effective light yield $L_{\rm eff}$ are used. Thick curves are based on the measurement [49], while thin curves are based on the alternative data set [50].

sensitive isotopes in CDMS ($^{73}$Ge) and XENON ($^{129}$Xe, $^{131}$Xe) have an unpaired neutron. Let us mention that in the proton case, also the COUPP [15] experiment provides a relevant constraint. However, it was not possible for us to implement a simulation of COUPP using the available information.

### B. A signal in CDMS?

Our default analysis of CDMS data uses the maximum gap method [48], which produces by construction only an upper limit on a DM signal. Let us now be somewhat more speculative and interpret the two events observed in the latest CDMS data as positive signal from DM scattering (see also [54]). In order to do this we use a model for the energy shape of the expected background from surface events. According to [3], this background is estimated by using the measured events in the $2\sigma$ window from their previous analysis, where no timing cut is yet imposed, see figure 3 of [47]. We count the number of events in the signal region and perform a fit to the energy distribution. Normalizing to the expected total number of background events (i.e. 0.8), we find $dN^{\rm bkgr}/dE_d = -0.00295 + 0.463/E_d$ where the recoil energy $E_d$ is in keVnr. Using this parameterization for the expected background shape we perform a fit to the two events by using the so-called extended maximum likelihood method [55].

In fig. 3 we show the CDMS allowed regions compared to the constraints from the other

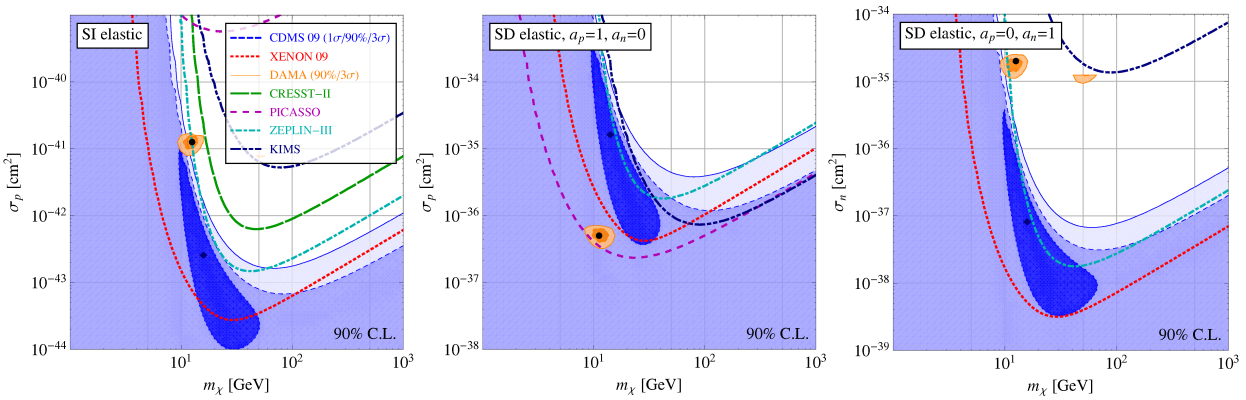


**FIG. 3**: Allowed regions for CDMS 2009 data ($1\sigma$, 90% and $3\sigma$ CL), DAMA (90% and $3\sigma$ CL), and constraints from other experiments (90% CL) for elastic SI scattering (left), SD scattering off protons (middle), and SD scattering off neutrons (right).

experiments for SI and SD elastic scattering. CDMS allowed regions are defined by $\Delta\chi^2 \equiv -2\log\mathcal{L}/\mathcal{L}^{\max}$ contours for 2 dof. We find that at $1\sigma$ CL a closed allowed region appears for CDMS ("positive signal"), while already at 90% CL only an upper bound is obtained. The CDMS favoured region is largely excluded by the XENON bound (and the PICASSO bound, in case of SD scattering off protons). In the case of SI scattering we have checked that in the combined fit to all all experiments except DAMA no closed region appears even at $1\sigma$, and we obtain only an upper limit.

We have also verified that in the case of inelastic scattering no closed region appears for CDMS. This follows from the fact that for inelastic scattering the signal is shifted to larger recoil energies, where CDMS sees no events, and therefore the data do not favour a positive signal. Hence, in the following we return to the conservative approach and use CDMS data only to set an upper limit on a DM signal using the maximum gap method.

### C. Inelastic SI and SD scattering

Let us now consider the assumption of inelastic DM scattering, put forward in ref. [18] in order to reconsile the DAMA signal with constraints from other experiments exploring the modified kinematics, see eq. (2) and the discussion given there. We start by first presenting results for the SI case, largely discussed in the literature, and then extend the inelastic scattering hypothesis also to SD interactions.

In order to identify possible solutions we have performed a combined analysis of all experiments, by adding the $\chi^2$ functions of the individual experiments. For those experiments which we analyse with the help of the maximum gap method (see sec. III) we proceed as follows. For a given point in the parameter space the probability obtained by the maximum gap method is converted into a $\Delta\chi^2$ by inverting the integral over the $\chi^2$-distribution for 2 dof. This "fake" $\Delta\chi^2$ is added to the one from the remaining experiments. Then we perform a scan over all three model parameters, $m_\chi$, $\sigma_p$, and $\delta$, in order to search for

local minima in the total $\chi^2$. While this recipe to incorporate the maximum gap method leads only to approximate confidence regions, it suffices for our purpose to locate potential solutions in the 3-dimensional parameter space.

Fig. 4 shows the results of such a scan for the SI case. We show projections of the 3-dimensional allowed regions onto the three 2-dimensional planes. We identify three local minima. The global minimum is $\chi^2_{\rm min,glob} = 10.0$ and is located at

$$\sigma_p = 2 \times 10^{-37}\,{\rm cm}^2\,, \quad m_\chi = 10.1\,{\rm GeV}\,, \quad \delta = 39\,{\rm keV}\,. \tag{9}$$

This solution corresponds to channeled events from iodine [25] and relies on the channeling calculations from [43] (scattering on sodium does not contribute to the signal, since the kinematics of inelastic scattering favor heavy over light nuclei). Furthermore this solution corresponds actually to a tiny, rather fine tuned region in $\delta$ and $m_\chi$. The values are choosen such that the minimal DM velocity $v_{\rm min}$ required to give a recoil energy of 3 keV needed to explain the DAMA signal is very close the galactic escape velocity. Indeed, the parameters are tuned such that the signal in DAMA is non-zero only in summer but zero in winter. This maximally enhances the modulated signal, while at the same time suppresses the unmodulated rate as well as the signal in the other experiments.[2] This is illustrated in the upper panel of fig. 4, where we show that the allowed region is located precisely between the contour curves for $v_{\rm min} = v_{\rm esc}$ in summer and in winter. Because of this fine tuning the best fit value for the cross section given in eq. (9) is very sensitive to the precise implementation of the DM halo profile and minor modifications in the analysis. This tuning of DM parameters $\delta$ and $m_\chi$ relative to properties of the galactic halo ($v_{\rm esc}$) is rather un-natural, and we consider this solution as being disfavoured despite the formally very good $\chi^2$ value. The same arguments apply for a local minimum around $\sigma_p = 10^{-36}\,{\rm cm}^2, m_\chi = 40\,{\rm GeV}, \delta = 130\,{\rm keV}$, corresponding to quenched events on iodine.

Another local minimum appears around $\sigma_p = 10^{-38}\,{\rm cm}^2, m_\chi = 50\,{\rm GeV}, \delta = 130\,{\rm keV}$ (light shaded regions in fig. 4). This corresponds to the conventional iDM solution discussed recently by many authors, e.g. [21–26]. This solution does not suffer from the fine tuning problem, but we find that it is disfavored with respect to the best fit with $\Delta\chi^2 = 16.1$. The reason are strong constraints mainly from CRESST, which is optimal for inelastic scattering since the heavy tungsten target nuclei allow for very efficient DM energy loss. In order to illustrate these constraints we show in fig. 5 allowed regions in the $\sigma_p, m_\chi$ plane for fixed values of $\delta$. The upper and lower left panels correspond to the SI fits with $\delta = 130$ keV and 40 keV, respectively. We observe that the $3\sigma$ DAMA region at $\delta = 130$ keV is completely excluded by the CRESST 90% CL bound and quite strongly constrained by several other experiments. The very thin strip corresponding to the DAMA region in the lower left plot illustrates the fine tuning problem. Furthermore, we observe that this solution is marginally compatible with the XENON bound.

Let us now move to the spin-dependent case. The results of the parameter scan of the combined $\chi^2$ is shown in fig. 6. We observe that the allowed regions are much larger than

[2] We remark that in such a case the fit to the DAMA modulated signal in terms of a cosine according to eq. (6) might not provide a good description, since the signal would correspond to a truncated cosine. We are not exploring such additional signatures here.

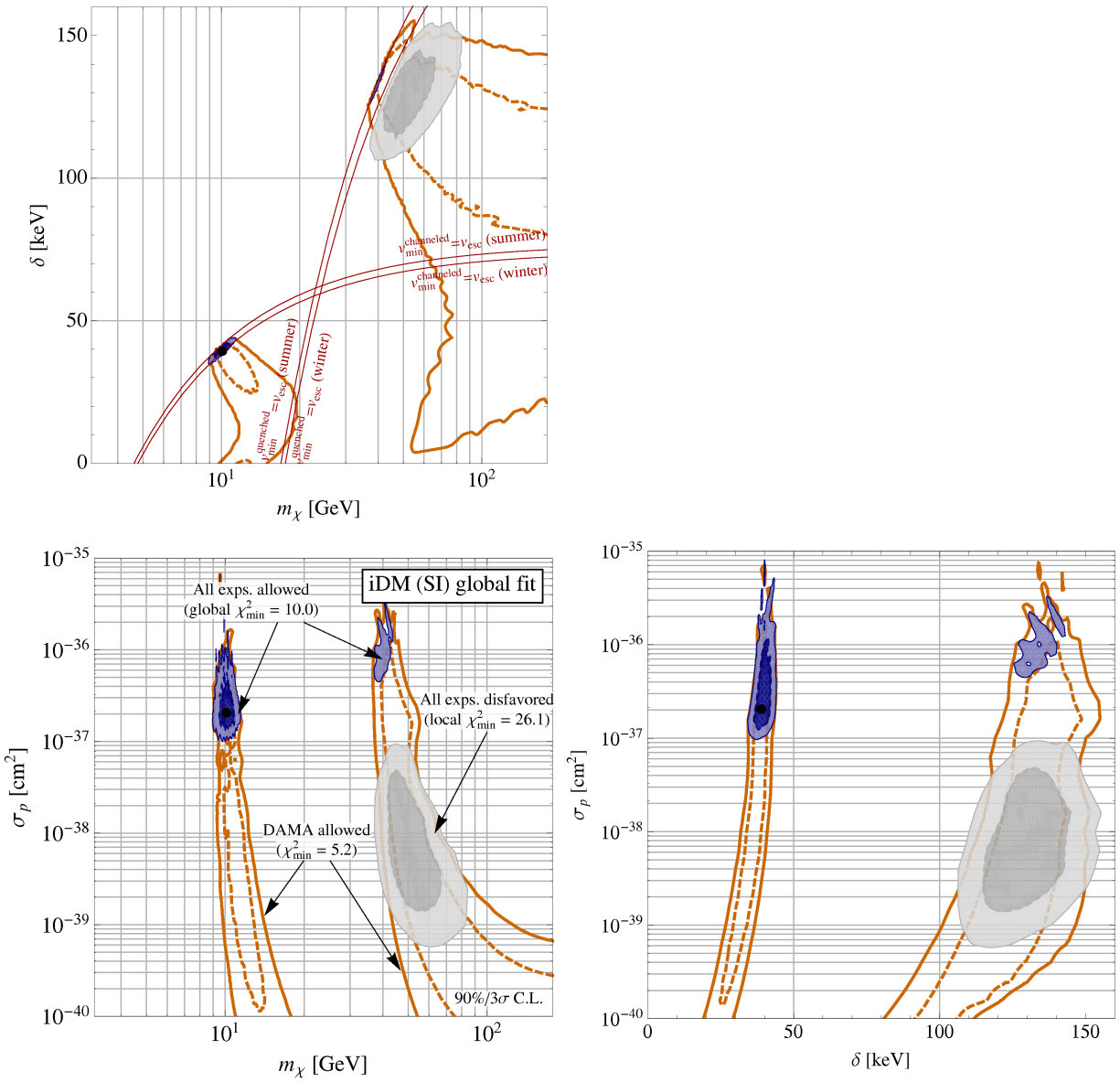


**FIG. 4**: Global fit of inelastic, spin-independent DM. We show projections of the 3-dimensional regions at 90% and $3\sigma$ CL onto the three 2-dimensional planes, by minimizing the global $\chi^2$ in each case with respect to the third (un-displayed) parameter. Confidence regions are defined for 2 dof. The fit includes CDMS (2008 + 2009 data), XENON (2009 analysis), DAMA, CRESST-II, ZEPLIN-III, and KIMS. The dark shaded regions are the allowed regions defined with respect to the global minimum, while the light shaded regions are defined relative to a local minimum, which by itself is disfavored relative to the global minimum with $\Delta\chi^2 = 16.1$. The open contours correspond to DAMA data only. In the upper panel we show also contours of $v_{\rm min} = v_{\rm esc} + v_{\rm earth}$ for a recoil energy of $E = 3$ keV, with and without quenching of iodine scatters, where $v_{\rm earth}$ is the velocity of the earth relative to the halo, depending on the time in the year.

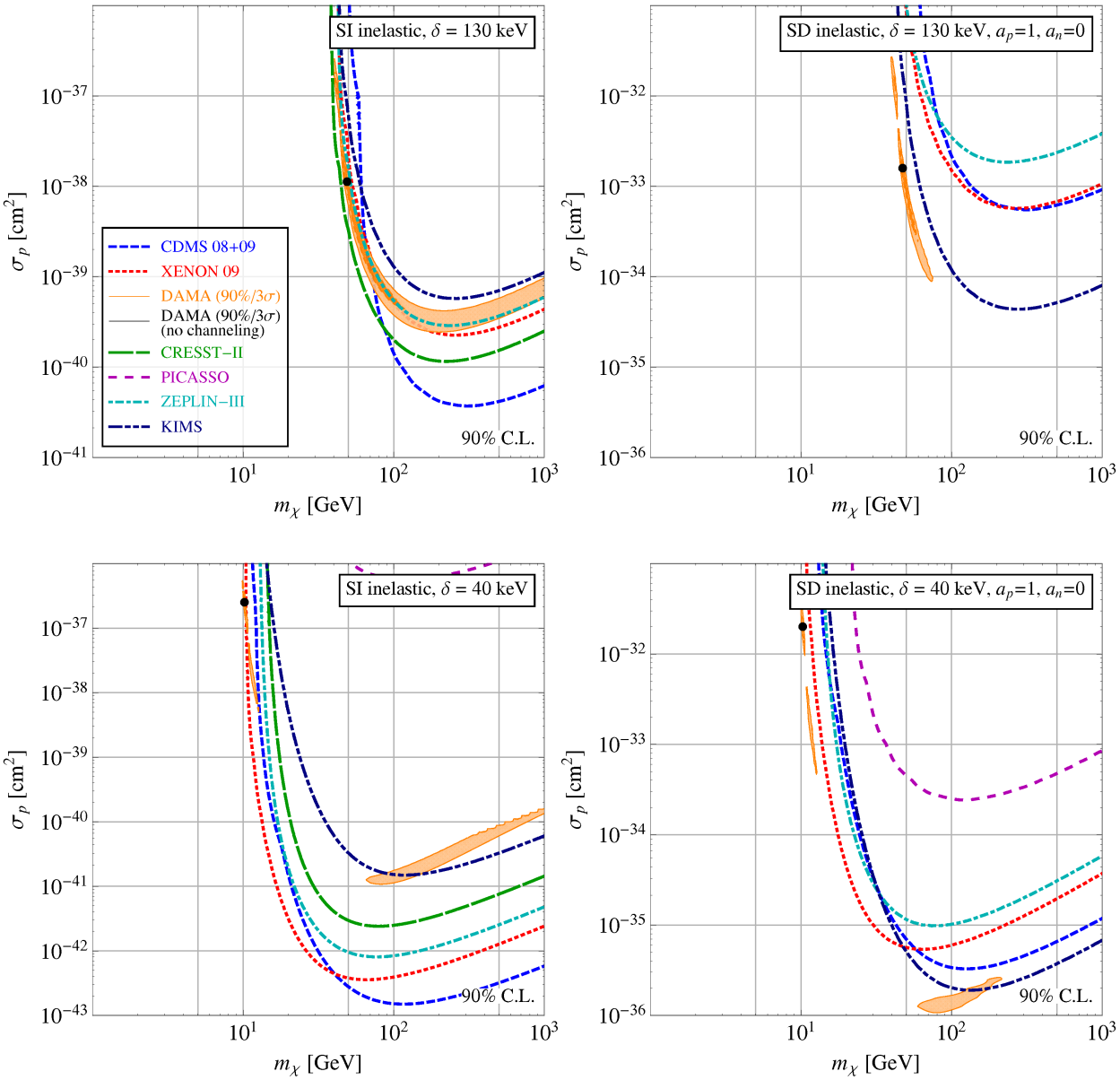


**FIG. 5**: DAMA allowed regions (90% and $3\sigma$ CL) and constraints from other experiments (90% CL) for inelastic DM scattering with SI interactions (left) and SD interactions with protons (right). We show regions in the $(m_\chi, \sigma_p)$ plane (2 dof) for fixed DM mass splitting $\delta$. The upper panels ($\delta = 130$ keV) correspond to a signal in DAMA from quenched events on iodine, whereas the lower panels ($\delta = 40$ keV) correspond to channeled events on iodine according to [43].

in the SI case. There are two different regions corresponding to fits of similar quality, corresponding to quenched events in DAMA and channeled events according to [43]:

$$m_\chi \simeq 40 - 70\,\mathrm{GeV}, \quad \delta \simeq 130\,\mathrm{keV} \qquad \text{(quenched events)} \tag{10}$$

$$m_\chi \simeq 10\,\mathrm{GeV}, \quad \delta \simeq 40\,\mathrm{keV} \qquad \text{(channeled events)} \tag{11}$$

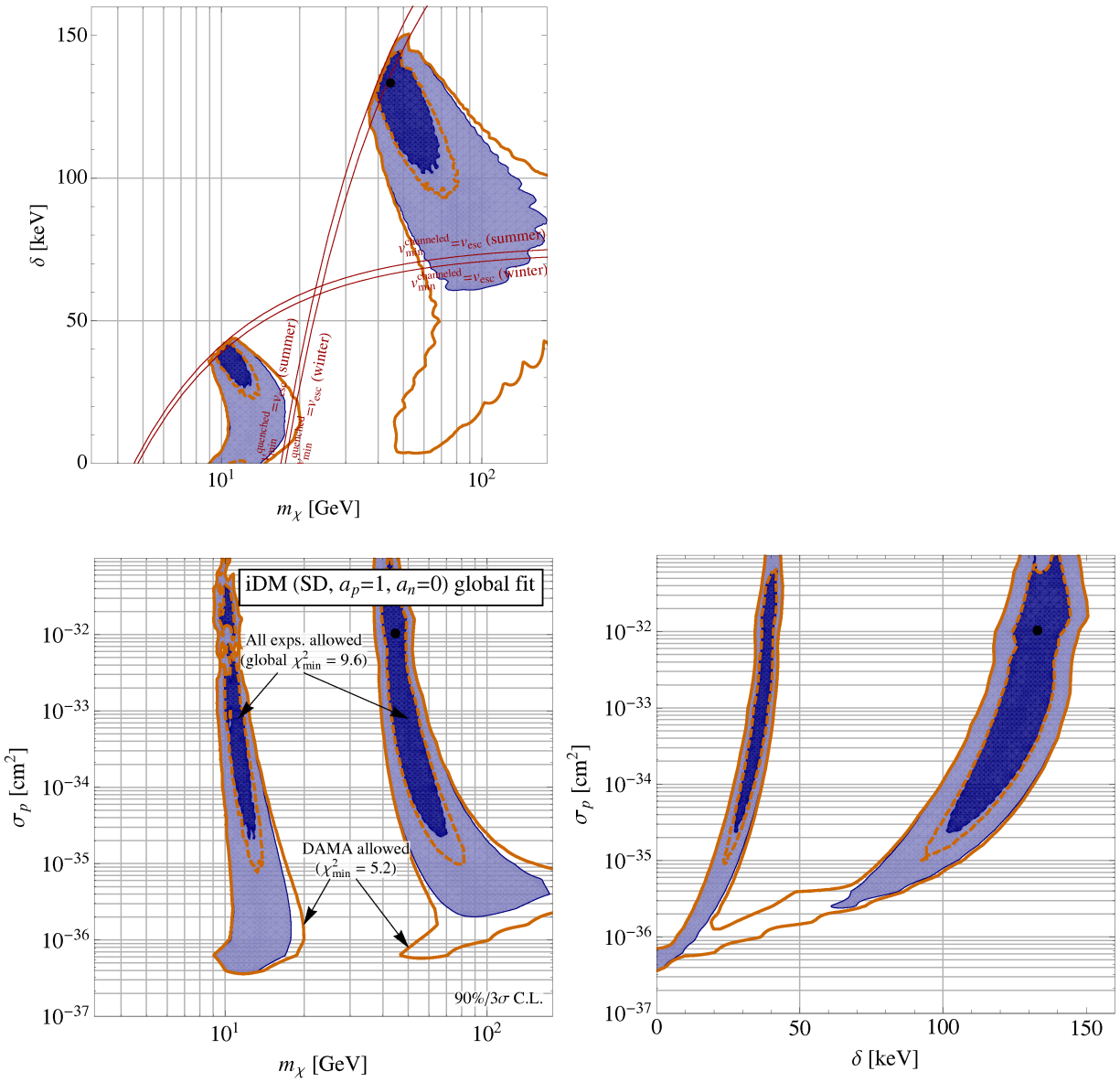


**FIG. 6**: Global fit of inelastic, spin-dependent DM. We show projections of the 3-dimensional regions at 90% and $3\sigma$ CL onto the three 2-dimensional planes, by minimizing the global $\chi^2$ in each case with respect to the third (un-displayed) parameter. Confidence regions are defined for 2 dof. The fit includes CDMS (2008 + 2009 data), XENON (2009 analysis), DAMA, CRESST-II, ZEPLIN-III, and KIMS. (We omit PICASSO which, due to the light target nucleus $^{19}$F has virtually no sensitivity to inelastic DM). The shaded regions refer to the global fit, whereas the open contours correspond to DAMA data only. In the upper panel we show also contours of $v_{\rm min} = v_{\rm esc} + v_{\rm earth}$ for a recoil energy of $E = 3$ keV, with and without quenching of iodine scatters, where $v_{\rm earth}$ is the velocity of the earth relative to the halo, depending on the time in the year.

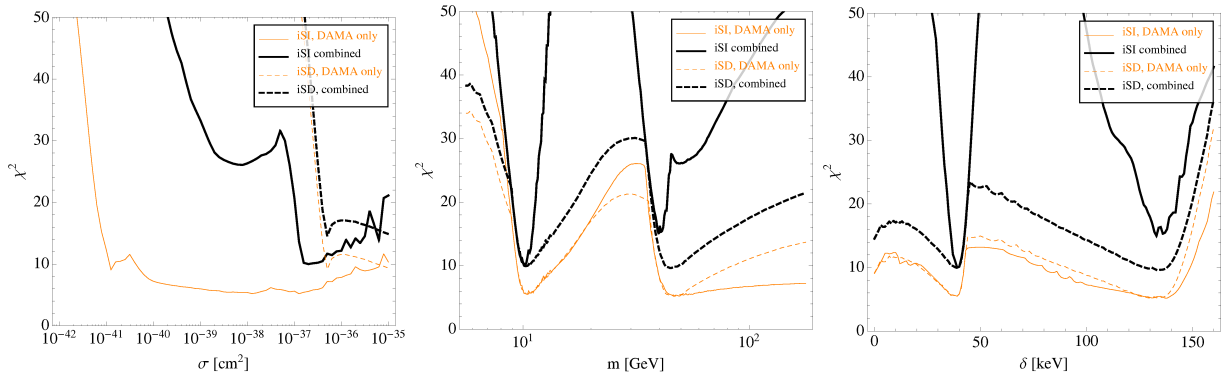


**FIG. 7**: $\chi^2$ projected onto the $\sigma_p, m_\chi$, and $\delta$ axes, where we minimize with respect to the two un-displayed parameters. We show the $\chi^2$ for DAMA data only (orange), and for the global data (black) assuming iSI interactions (solid) and iSD interactions on protons (dashed).

with cross sections in a wide range of few $\times\, 10^{-35}\,\mathrm{cm}^2 \lesssim \sigma_p \lesssim$ few $\times\, 10^{-32}\,\mathrm{cm}^2$. The right panels of fig. 5 show that the allowed regions are safely compatible with the constraints from all other experiments. The explanation is as follows: the SD coupling to protons drastically reduces the power of even $Z$ target experiments (XENON, CDMS), while the inelastic kinematics strongly disfavour light targets (PICASSO), which provide a main challenge for DAMA in the elastic SD case, see fig. 1.

It is, however, important to remark that for each fixed $\delta$, it is only a very small range of $m_\chi$ that gives a good fit to the DAMA data. Varying $m_\chi$ by a small amount requires a large change of the cross section to maintain a good fit, see fig. 5 right panels. This is because the scattering is sensitive to the exponentially suppressed tail of the DM velocity distribution close to $v_{\rm esc}$. However, in contrast to the SI case, we observe from the top panel of fig. 6 the 90% CL regions extend relatively far way from the $v_{\rm min} = v_{\rm esc}$ curves. Hence, the iSD case does require a relatively precise tuning of model parameters $(\sigma_p, m_\chi, \delta)$ among themselves, but the tuning with respect to astrophysics is not necessary here. Therefore, if we assume the spin-dependent inelastic scenario to be true, the results can be interpreted as reflecting very high sensitivity of direct detection experiments to the model parameters up to astrophysical uncertainties.

Let us mention that we have not been able to include data from the COUPP [15] experiment in our analysis, due to missing information. In contrast to the elastic SD case we do not expect that COUPP will provide a relevant constraint in the inelastic case. Namely, the scattering on $^{19}$F is negligibe due to its small mass, in the same way as for PICASSO. The constraint from iodine contained in their $CF_3I$ target should also be much weaker than the one coming from KIMS due to the much larger exposure of the latter (3409 kg days for KIMS vs. 250 kg days for COUPP). We do not show the results for iSD scattering off neutrons, but we have checked that for the same reasons as in the elastic case, the DAMA region is safely excluded by constraints from XENON and CDMS.

To conclude this section, we show in fig. 7 the projections of the DAMA-only and global $\chi^2$ function for the three parameters $\sigma_p, m_\chi, \delta$, separately, for the iSI as well as iSD scenarios.

## V. A SIMPLE MODEL

As we have seen in the previous section, the possibility that DM scatters inelastically with spin-dependent cross section provides a viable explanation for the DAMA signal that simultaneously avoids the bounds from the other direct detection experiments. We now show that iSD scattering can be realized in concrete models.

It actually does not require too much work to find such a model. To be concrete let us start with fermionic DM that interacts with the visible matter through the effective interaction

$$\mathcal{L}_{\rm int} = \frac{1}{\Lambda^2}\left[\bar{\psi}\Gamma_{\rm DM}\psi\right]\left[\bar{q}\Gamma_{\rm vis}q\right], \tag{12}$$

where $\Gamma_{\rm DM,vis}$ denote the Dirac structure of the four-fermion operator which we keep general for now, $\psi = (\eta, \xi^\dagger)$ is a Dirac fermion (for two-component spinors we use the notation of [56]) and $q$ are the light quark fields. We could have equally well chosen couplings to leptons, in which case the analysis of DAMA would have followed ref. [29]. The above effective interaction can arise from an exchange of heavy mediators with mass $\mathcal{O}(\Lambda)$ under which both visible and DM fermions are charged. In [18] the four-fermion interaction (12) was chosen to be of the $V\otimes V$ form (i.e., $\Gamma_{\rm DM} = \gamma_\mu, \Gamma_{\rm vis} = \gamma^\mu$). This gives a spin-independent scattering cross section for inelastic DM. We show below that tensor interactions give spin-dependent inelastic scattering instead. To the best of our knowledge this realization has not been discussed in the context of inelastic DM scattering in the literature before (for some particle physics realizations of inelastic DM see [23, 24, 57–62]).

If $\psi$ is a Dirac fermion, the interaction (12) leads to elastic scattering. However, if in addition to the Dirac mass term $m\bar{\psi}\psi$ there are also Majorana mass terms $(\delta_\eta\eta\eta + \delta_\xi\xi\xi)/2$, then the Dirac fermion splits into two Majorana fermions with masses $m \pm \delta$ (for simplicity let us take $\delta_\eta = \delta_\xi = \delta$). The mass eigenstates are [18]

$$\chi_1 = \frac{i}{\sqrt{2}}(\eta - \xi), \qquad \chi_2 = \frac{1}{\sqrt{2}}(\eta + \xi). \tag{13}$$

It is reasonable to assume that $\delta \ll m$, since Majorana mass terms break a global symmetry, while the Dirac mass term conserves it. This is exactly the hierarchy needed phenomenologically, since $m \sim \mathcal{O}(100\ \text{GeV})$, $\delta \sim \mathcal{O}(100\ \text{keV})$ are needed for DAMA.

Let us now assume that the four-fermion interaction between DM and the visible sector (12) is of $T\otimes T$ form,

$$\mathcal{L}_{\rm int} = \frac{C_{\rm T}}{\Lambda^2}\left[\bar{\psi}\Sigma_{\mu\nu}\psi\right]\left[\bar{q}\Sigma^{\mu\nu}q\right], \tag{14}$$

where $\Sigma^{\mu\nu} = i[\gamma^\mu, \gamma^\nu]/2$. From the relations $\chi_i\sigma^{\mu\nu}\chi_j = -\chi_j\sigma^{\mu\nu}\chi_i$, $\chi_i^\dagger\bar{\sigma}^{\mu\nu}\chi_j^\dagger = -\chi_j^\dagger\bar{\sigma}^{\mu\nu}\chi_i^\dagger$ (see e.g. [56]), it follows that for Majorana fermions the diagonal tensor operator vanishes.[3] Thus, one finds for the DM tensor current

$$\bar{\psi}\Sigma_{\mu\nu}\psi = -2i(\chi_2\sigma_{\mu\nu}\chi_1 + \chi_2^\dagger\bar{\sigma}_{\mu\nu}\chi_1^\dagger), \tag{15}$$

[3] Here, $\sigma^{\mu\nu} \equiv i(\sigma^\mu\bar{\sigma}^\nu - \sigma^\nu\bar{\sigma}^\mu)/4$, $\bar{\sigma}^{\mu\nu} \equiv i(\bar{\sigma}^\mu\sigma^\nu - \bar{\sigma}^\nu\sigma^\mu)/4$, and $\sigma^\mu = (1, \sigma^i)$, $\bar{\sigma}^\mu = (1, -\sigma^i)$, with $\sigma^i$ the Pauli matrices.

which leads to inelastic scattering for $\delta \neq 0$. Furthermore, it is well known that in the nonrelativistic limit the $T \otimes T$ interaction leads to spin dependent scattering, see e.g. [63]. For instance, in our case the matrix element for $\chi_1 \to \chi_2$ scattering on a nucleus $N$ has the form $\langle N|\bar{q}S_i q|N\rangle(\zeta^\dagger_{2,s'}\sigma_i\zeta_{1,s})$, with $S_i$ the spin operator and $\zeta_{2,s'}, \zeta_{1,s}$ the nonrelativistic two-component spinor wave functions for the DM particles.

It is important to note that the $T \otimes T$ current is the only chiral structure that leads to spin-dependent inelastic scattering in the above simple model of two Majorana fermions split by small Majorana mass terms. The $T \otimes TA$ structure of the four-fermion interaction would vanish in the $v \to 0$ limit, while the $TA \otimes TA$ interaction is equivalent to $T \otimes T$ as is easily checked from the definition of $\gamma_5$. The $V \otimes V$ product leads to SI inelastic scattering [18], $A \otimes A$ to SD elastic scattering, the $V \otimes A$ product vanishes in the nonrelativistic limit, while the scalar and pseudoscalar couplings obviously do not lead to spin dependent interactions.

One still has the freedom to choose appropriate values for Wilson coefficients $C_T$ for different flavors of the quark current, i.e. the couplings to $u$ and $d$ quarks. In section IV we explored two extreme cases where the coupling is proportional to the charge (so that DM scatters only on protons) or that the coupling to $d$ is twice as large and opposite to the coupling to $u$ quarks (so that DM scatters only on neutrons). From the fits the first option is preferred.

One can also construct a model with DM that is a scalar and that has inelastic spin-dependent scattering on visible matter. But this interaction is inevitably suppressed by the nonrelativistic DM velocity because of the derivative in the DM current and thus less realistic phenomenologically in light of relatively large scattering cross sections needed to fit DAMA.

## VI. CONCLUSIONS

The CDMS-II collaboration has recently reported the observation of two events, with an expected background of 0.9 events [3], by about doubling the exposure with respect to previous results. We have performed a combined analysis of direct DM searches including the claimed signal by DAMA [1, 2], the recent CDMS-II results, as well as a re-analysis of XENON10 data. We have considered four classes of possible WIMP-nucleus scattering models: elastic (e) or inelastic (i) scattering and spin-dependent (SD) or spin-independent (SI) scattering. This covers a large set of DM models. While three types of WIMP-nucleus scattering have already been considered in the literature (i.e., eSD, eSI, and iSI scattering), our analysis is the first to also include the fourth possibility — the inelastic spin dependent scattering. In fact it is this latter possibility that can simultaneously explain the DAMA signal and avoid bounds from the other direct detection experiments as we demonstrated in the present paper.

For eSI scattering the DAMA region is safely excluded by data from XENON10, based on a recent re-analysis of their data [5], mainly due to a lower energy threshold, while for the eSD case DAMA is in conflict with the bound from PICASSO. For iSI scattering we find two possible solutions. The traditional "iDM" region with $m_\chi \simeq 50$ GeV and $\delta \simeq 130$ keV is disfavoured by CRESST-II data and further constrained by CDMS-II. A low mass region exists around $m_\chi \simeq 10$ GeV and $\delta \simeq 40$ keV. It requires, however, the presence of the channeling effect in DAMA, and leads to rather severe tuning of the DM mass and mass-

splitting with respect to the properties of the galactic DM halo, such that the WIMP velocity distribution is sampled precisely around the escape velocity.

For the iSD case, on the other hand, we do find allowed regions of the parameter space such that the signal in DAMA is explained, while there is no conflict with any of the other experiments for non-vanishing couplings to protons and suppressed couplings to neutrons. The solution suffers from some tuning among the DM parameters $\sigma_p, m_\chi$, and $\delta$ (which a priori is not a problem, but just indicates very high sensitivity of the experiments to these parameters), while they do not require a very precise tuning with respect to the escape velocity. The required DM parameters for the two solutions are $m_\chi$ around 40–70 GeV, $\delta \simeq 130$ keV (corresponding to quenched events in DAMA), and $m_\chi \simeq 10$ GeV, $\delta \simeq 40$ keV (which relies on the channeling effect). Cross sections are found in a wide range of few $\times\, 10^{-35}\,\mathrm{cm}^2 \lesssim \sigma_p \lesssim$ few $\times\, 10^{-32}\,\mathrm{cm}^2$. We presented also a simple toy model, showing how to realize iSD scattering in a specific framework.

In the case of elastic scattering, we also adopted a somewhat speculative approach to the recent CDMS-II data, and have performed a maximum likelihood fit to the two events. We find that at $1\sigma$ CL a closed allowed region appears for CDMS ("positive signal"), while already at 90% CL only an upper bound is obtained. The CDMS favoured region is largely excluded by the XENON bound (and the PICASSO bound, in case of SD scattering off protons). In a combined analysis of CDMS and the exclusion limits from other experiments, the "signal" becomes less than $1\sigma$. More information on this can be expected soon from XENON-100 [64].

## Note added in proofs

After this work was completed, we were able to perform a fit to the data from the COUPP experiment. This was made possible by kind assistance from the COUPP collaboration, especially Juan I. Collar, who provided crucial data on the bubble formation threshold energies. We have checked that COUPP limits are subdominant in the case of eSI, iSI, and iSD scattering. For eSD scattering, COUPP improves the PICASSO limit by up to a factor of 2 in $\sigma_p$ for $m_\chi \gtrsim 50$ GeV.


### Acknowledgments

We would like to thank Jernej Kamenik for useful discussions. JK would like to thank the Max-Planck-Institute for Nuclear Physics for an enjoyable visit and kind hospitality during part of this work. Fermilab is operated by Fermi Research Alliance, LLC under Contract No. DE-AC02-07CH11359 with the US Department of Energy. This work was partly supported by the Sonderforschungsbereich TR 27 "Neutrinos and Beyond" of the Deutsche Forschungsgemeinschaft. The work of JZ is supported in part by the European Commission RTN network, Contract No. MRTN-CT-2006-035482 (FLAVIAnet) and by the Slovenian Research Agency.

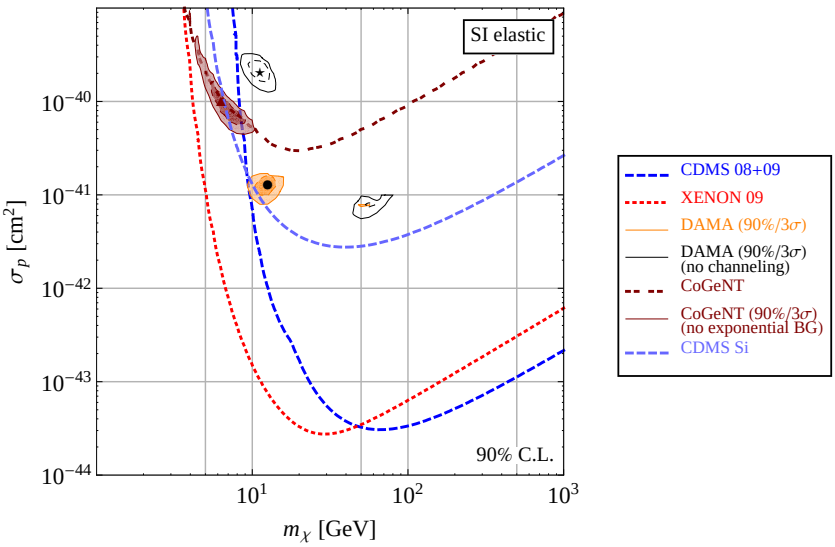


**FIG. 8**: CoGeNT and DAMA allowed regions (90% and $3\sigma$ CL) and constraints from other experiments (90% CL) for elastic spin-independent scattering. Shaded DAMA regions have been obtained assuming channeling according to [43], while the black contours correspond to no channeling. The CoGeNT upper bound follows from a fit including an exponential background, while the allowed region is obtained when the exponential is removed from the background model.

### Appendix A: Interpretation of CoGeNT results

After publication of this manuscript, the CoGeNT collaboration has published results from the initial run of their ultra low noise germanium detector in the Soudan Underground Laboratory [65]. The detector has a very low energy threshold of 0.4 keVee, the lowest achieved so far by any dark matter experiment. The data from an eight week exposure of the detector with a fiducial mass of 330 g reveals $\sim$ 100 events near the low-energy threshold for which the collaboration was not able to identify a background source. The "signal" is consistent with an exponential background. It is, however, also compatible with the hypothesis of an $\mathcal{O}(10$ GeV) WIMP. Below we show that this hypothesis is strongly disfavored by other experiments, though not completely ruled out.

In the analysis we assume standard astrophysical parameters for the dark matter halo, see Section II. In the fit we use the data from Fig. 3 of [65] in the 0.4–3.2 keVee energy range. For the quenching factors we use the approximate formula (based on [66], Eq. (2.6), with $\kappa = 0.2$ [67])

$$\frac{2}{1+\sqrt{1+15.55/E}}\,, \tag{A1}$$

where E is the energy in keVee. Whether or not one finds in the fit a DM signal depends crucially on the assumed background. We perform fits for two different background models: (i) a 7-parameter model consisting of a constant (1 parameter), an exponential (2 parameters), and two Gaussians at the known positions of the $^{68}$Ge and $^{65}$Zn lines ($2 \times 2$ parameters); this background model is similar to the one used by the CoGeNT collaboration. (ii) A

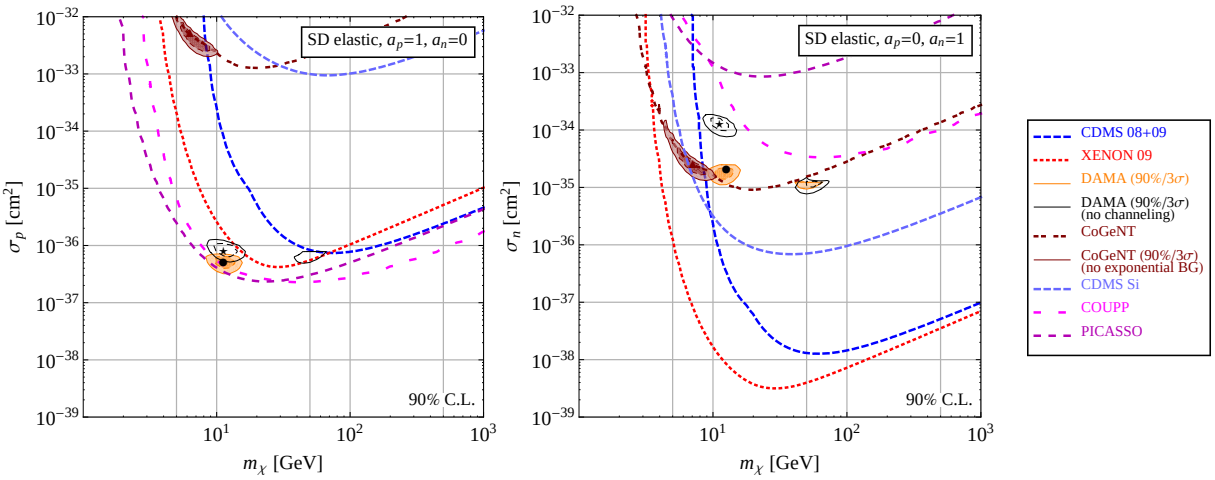


**FIG. 9**: CoGeNT and DAMA allowed regions (90% and $3\sigma$ CL) and constraints from other experiments (90% CL) for SD scattering on protons (left) and on neutrons (right). See also caption of Fig. 8.

similar background model, but without the exponential. The results are shown in Fig. 8 for elastic SI scattering, and in Fig. 9 for elastic SD scattering. We also include fits to the data from the CDMS Silicon detectors (labeled CDMS-Si) [68, 69]. In the SD case, we use the structure functions for $^{29}$Si as given in [40].

For the full 7-parameter background model only an upper limit on the WIMP cross-section is obtained for both SI and SD scattering. It is only if one assumes that the background does not contain an exponential component that a closed allowed region appears in the $m_\chi - \sigma_p$ plane, with $m_\chi \sim 5 - 10$ GeV, $\sigma_p \sim 10^{-4}$ pb for SI scattering, and $\sigma_p \sim 10^4$ pb ($\sigma_n \sim 10$ pb) for SD scattering on protons (neutrons). In the case of SD scattering on neutrons, the CoGeNT-preferred region overlaps with the DAMA-preferred region. For SI scattering, marginal overlap between CoGeNT and DAMA could be achieved if the fraction of channeled events is assumed to be smaller than what was assumed by the DAMA collaboration (orange shaded contours), but larger than zero (black contours). Also, an admixture of an exponential background to a DM signal in CoGeNT could shift the allowed region to lower values of $\sigma_p$, closer to the DAMA allowed region. However, without a clear prediction for the background all such modifications are mere speculations. Furthermore, both the DAMA allowed region and the CoGeNT "signal" region are ruled out at 90% CL by the other experiments for the standard choices of experimental parameters. XENON-10 and CDMS-Si rule out the SI case as well as SD scattering on neutrons, while COUPP and PICASSO rule out SD scattering on protons as an explanation for CoGeNT and/or DAMA, cf. Figs. 8 and 9. As fig. 2 shows, relaxing the assumptions on the effective light yield $L_{\rm eff}$ in XENON-10 can make XENON-10 and CoGeNT (but not DAMA) marginally compatible at 90% C.L. We have also checked that CoGeNT results do not further constrain inelastic DM (whether SI or SD) discussed in Section IV C.

In conclusion, we find that the background only hypothesis gives an excellent fit to the CoGeNT data, while a DM interpretation of this data is disfavored by other experiments.

We differ in this conclusion from the authors of [70], who find that CoGeNT and DAMA are consistent with the remaining experiments. This difference may be traced back to the treatment of $L_{\rm eff}$ for XENON-10. The authors of [70] assume the true $L_{\rm eff}$ to lie at the lower end of the 1-$\sigma$ error bars of the most conservative measurement available [50]. Given the discrepancy between different measurements of $L_{\rm eff}$, the possibility of such a systematic shift cannot be excluded until systematical errors in the $L_{\rm eff}$ measurement are better understood. Other differences between our analysis and that of [70] are in the choice of DM halo parameters and in that the authors of [70] demand that the background does not exceed the DM signal, while we allow both to float freely.

---


[1] R. Bernabei et al., Riv. Nuovo Cim. **26N1**, 1 (2003), astro-ph/0307403.
[2] R. Bernabei et al. (DAMA), Eur. Phys. J. **C56**, 333 (2008), 0804.2741.
[3] Z. Ahmed et al. (CDMS) (2009), 0912.3592.
[4] J. Angle et al. (XENON), Phys. Rev. Lett. **100**, 021303 (2008), 0706.0039.
[5] J. Angel et al. (XENON) (2009), 0910.3698.
[6] A. Bottino, F. Donato, N. Fornengo, and S. Scopel, Phys. Rev. **D77**, 015002 (2008), 0710.0553.
[7] A. Bottino, F. Donato, N. Fornengo, and S. Scopel, Phys. Rev. **D78**, 083520 (2008), 0806.4099.
[8] F. Petriello and K. M. Zurek, JHEP **09**, 047 (2008), 0806.3989.
[9] J. L. Feng, J. Kumar, and L. E. Strigari, Phys. Lett. **B670**, 37 (2008), 0806.3746.
[10] S. Chang, A. Pierce, and N. Weiner, Phys. Rev. **D79**, 115011 (2009), 0808.0196.
[11] M. Fairbairn and T. Schwetz, JCAP **0901**, 037 (2009), 0808.0704.
[12] C. Savage, G. Gelmini, P. Gondolo, and K. Freese, JCAP **0904**, 010 (2009), 0808.3607.
[13] Y. G. Kim and S. Shin, JHEP **05**, 036 (2009), 0901.2609.
[14] B. Feldstein, A. L. Fitzpatrick, E. Katz, and B. Tweedie (2009), 0910.0007.
[15] E. Behnke et al. (COUPP), Science **319**, 933 (2008), 0804.2886.
[16] H. S. Lee. et al. (KIMS), Phys. Rev. Lett. **99**, 091301 (2007), 0704.0423.
[17] S. Archambault et al. (PICASSO), Phys. Lett. **B682**, 185 (2009), 0907.0307.
[18] D. Tucker-Smith and N. Weiner, Phys. Rev. **D64**, 043502 (2001), hep-ph/0101138.
[19] G. Angloher et al. (CRESST-II) (2008), 0809.1829.
[20] D. B. Cline, W. Ooi, and H. Wang (2009), 0906.4119.
[21] S. Chang, G. D. Kribs, D. Tucker-Smith, and N. Weiner, Phys. Rev. **D79**, 043513 (2009), 0807.2250.
[22] J. March-Russell, C. McCabe, and M. McCullough, JHEP **05**, 071 (2009), 0812.1931.
[23] Y. Cui, D. E. Morrissey, D. Poland, and L. Randall, JHEP **05**, 076 (2009), 0901.0557.
[24] C. Arina, F.-S. Ling, and M. H. G. Tytgat, JCAP **0910**, 018 (2009), 0907.0430.
[25] K. Schmidt-Hoberg and M. W. Winkler, JCAP **0909**, 010 (2009), 0907.3940.
[26] C. Savage, K. Freese, P. Gondolo, and D. Spolyar, JCAP **0909**, 036 (2009), 0901.2713.
[27] R. Foot, Phys. Rev. **D78**, 043529 (2008), 0804.4518.
[28] E. Masso, S. Mohanty, and S. Rao, Phys. Rev. **D80**, 036009 (2009), 0906.1979.
[29] J. Kopp, V. Niro, T. Schwetz, and J. Zupan, Phys. Rev. **D80**, 083502 (2009), 0907.3159.
[30] Y. Bai and P. J. Fox, JHEP **11**, 052 (2009), 0909.2900.
[31] B. Feldstein, A. L. Fitzpatrick, and E. Katz (2009), 0908.2991.

[32] S. Chang, A. Pierce, and N. Weiner (2009), 0908.3192.
[33] D. E. Kaplan, G. Z. Krnjaic, K. R. Rehermann, and C. M. Wells (2009), 0909.0753.
[34] M. Kuhlen et al. (2009), 0912.2358.
[35] M. Lisanti and J. G. Wacker (2009), 0911.4483.
[36] M. Lisanti and J. G. Wacker (2009), 0911.1997.
[37] P. Ullio, M. Kamionkowski, and P. Vogel, JHEP **07**, 044 (2001), hep-ph/0010036.
[38] G. Jungman, M. Kamionkowski, and K. Griest, Phys. Rept. **267**, 195 (1996), hep-ph/9506380.
[39] P. Toivanen, M. Kortelainen, J. Suhonen, and J. Toivanen, Phys. Rev. **C79**, 044302 (2009).
[40] V. A. Bednyakov and F. Simkovic, Phys. Part. Nucl. **37**, S106 (2006), hep-ph/0608097.
[41] R. Bernabei et al., Phys. Lett. **B389**, 757 (1996).
[42] E. M. Drobyshevski, Mod. Phys. Lett. **A23**, 3077 (2008), 0706.3095.
[43] R. Bernabei et al., Eur. Phys. J. **C53**, 205 (2008), 0710.0288.
[44] J. Graichen, K. Maier, J. Schuth, A. Siepe, and W. von Witsch, Nucl. Instrum. Meth. **A485**, 774 (2002).
[45] G. B. Gelmini (2009), 0910.3032.
[46] V. A. Kudryavtsev, M. Robinson, and N. J. C. Spooner (2009), 0912.2983.
[47] Z. Ahmed et al. (CDMS), Phys. Rev. Lett. **102**, 011301 (2009), 0802.3530.
[48] S. Yellin, Phys. Rev. **D66**, 032005 (2002), physics/0203002.
[49] P. Sorensen et al., Nucl. Instrum. Meth. **A601**, 339 (2009), 0807.0459.
[50] A. Manzur et al. (2009), 0909.1063.
[51] V. N. Lebedenko et al., Phys. Rev. **D80**, 052010 (2009), 0812.1150.
[52] H. Kim, talk at Accelerator and Particle Physics Institute (APPI2002), February 13 - 16, 2002, Iwate, Japan, available at http://acfahep.kek.jp/appi/2002/proceedings.html.
[53] H. S. Lee. et al. (KIMS), Phys. Rev. Lett. **99**, 091301 (2007), 0704.0423.
[54] A. Bottino, F. Donato, N. Fornengo, and S. Scopel (2009), 0912.4025.
[55] R. Barlow, Nucl. Instrum. Meth. **A297**, 496 (1990), ISSN 0168-9002.
[56] H. K. Dreiner, H. E. Haber, and S. P. Martin (2008), 0812.1594.
[57] N. Arkani-Hamed, L. J. Hall, H. Murayama, D. Tucker-Smith, and N. Weiner, Phys. Rev. **D64**, 115011 (2001), hep-ph/0006312.
[58] D. S. M. Alves, S. R. Behbahani, P. Schuster, and J. G. Wacker (2009), 0903.3945.
[59] B. Batell, M. Pospelov, and A. Ritz, Phys. Rev. **D79**, 115019 (2009), 0903.3396.
[60] A. Katz and R. Sundrum, JHEP **06**, 003 (2009), 0902.3271.
[61] C. Cheung, J. T. Ruderman, L.-T. Wang, and I. Yavin, Phys. Rev. **D80**, 035008 (2009), 0902.3246.
[62] M. Kadastik, K. Kannike, A. Racioppi, and M. Raidal (2009), 0912.3797.
[63] A. Kurylov and M. Kamionkowski, Phys. Rev. **D69**, 063503 (2004), hep-ph/0307185.
[64] E. Aprile and L. Baudis (XENON100) (2009), 0902.4253.
[65] C. E. Aalseth et al. (CoGeNT) (2010), 1002.4703.
[66] H. Chagani, P. Majewski, E. J. Daw, V. A. Kudryavtsev, and N. J. C. Spooner, JINST **3**, 06003 (2008), 0806.1916.
[67] P. S. Barbeau, J. I. Collar, and O. Tench, JCAP **0709**, 009 (2007), nucl-ex/0701012.
[68] D. S. Akerib et al. (CDMS), Phys. Rev. Lett. **96**, 011302 (2006), astro-ph/0509259.
[69] D. S. Akerib et al. (CDMS), Phys. Rev. **D73**, 011102 (2006), astro-ph/0509269.
[70] A. L. Fitzpatrick, D. Hooper, and K. M. Zurek (2010), 1003.0014.